Impact of trapping on tritium self-sufficiency and tritium inventories in fusion power plant fuel cycles

PAPER • OPEN ACCESS

Impact of trapping on tritium self-sufficiency and tritium inventories in fusion power plant fuel cycles

To cite this article: Samuele Meschini *et al* 2025 *Nucl. Fusion* **65** 036010

OPEN ACCESS
IOP Publishing | International Atomic Energy Agency
Nuclear Fusion
Nucl. Fusion **65** (2025) 036010 (16pp)
https://doi.org/10.1088/1741-4326/adacfa

Impact of trapping on tritium self-sufficiency and tritium inventories in fusion power plant fuel cycles

Samuele Meschini[1,*], **Rémi Delaporte-Mathurin**[1], **George R. Tynan**[1,2] and **Sara E. Ferry**[1]

[1] Plasma Science and Fusion Center, Massachusetts Institute of Technology, Cambridge, MA 02139, United States of America
[2] Department of Mechanical and Aerospace Engineering and The Center for Energy Research, University of California, San Diego, CA, United States of America

E-mail: sam_mesc@mit.edu

Received 12 September 2024, revised 4 December 2024
Accepted for publication 22 January 2025
Published 11 February 2025

Abstract

The dynamic analysis of fusion power plant (FPP) fuel cycles highlights the challenge of achieving tritium self-sufficiency in future FPPs. While state-of-the-art fuel cycle models offer valuable insights into the necessary design parameters for attaining tritium self-sufficiency, none of these models currently consider the impact of tritium trapping within fuel cycle components. However, detailed analysis of individual components reveals that substantial amounts of tritium can be trapped within the first wall, divertors, and breeding blanket systems, suggesting that tritium trapping may significantly influence the FPP ability to achieve self-sufficiency. The compounded effects of additional tritium traps generated by irradiation effects and component replacements further exacerbate this challenge. The novelty of this work is the integration of an explicit, physics-based model for tritium trapping, evolution of damage-induced traps, and component replacements into a dynamic, system-level model of a fuel cycle. The results show an increase of a factor $10^3 - 10^4$ of tritium inventory in the first wall and vacuum vessel of an ARC-class FPP when accounting for the aforementioned phenomena. This, coupled with the replacement of components subject to significant tritium trapping, slows down fuel cycle dynamics, resulting in an extended tritium doubling time (50% increase), higher start-up inventory (30% increase), and higher required tritium breeding ratio (2%–5%) compared to a scenario without tritium trapping.

Keywords: fuel cycle, tritium trapping, tritium self-sufficiency, tritium inventories, maintenance, tritium breeding

(Some figures may appear in colour only in the online journal)

* Author to whom any correspondence should be addressed.

1. Introduction

The first generation of fusion power plants (FPPs) will face a limited tritium supply and must be able to breed sufficient tritium to self-fuel, have tritium in reserve, and provide startup tritium to new FPPs. FPPs will seek to balance efficient tritium breeding with the minimization of on-site tritium inventory. The renewed interest in commercial fusion energy has spurred new development activities in regards to fusion fuel cycle technology and modeling [1, 2].

Recent fuel cycle models have been developed for various FPP designs, such as ARC [3], DEMO [4, 5], STEP [3], and CFETR [6]. A common outcome of these works is that achieving tritium self-sufficiency is considerably more complicated than simply attaining a tritium breeding ratio (TBR) of unity in the breeding blanket ('blanket'). Engineering constraints, system dynamics, and plant performance targets for a given FPP design typically result in a required TBR significantly greater than unity (often in the range of 1.1–1.4). Since a given FPP with a given blanket and shielding design has a maximum achievable TBR, it is very important to have an accurate understanding of the overall fuel cycle dynamics of the FPP early in the design process to ensure the chosen blanket is sufficient. Fuel cycle models that oversimplify relevant phenomena or overlook important loss terms can lead to an FPP design that is unable to become tritium self-sufficient once built.

Notably, existing fuel cycle models neglect, or account for it in a very simplified way, the phenomenon of tritium trapping. Hydrogen trapping in materials occurs when mobile hydrogen atoms become stuck at trapping sites within the material lattice, such as interstitials, defects, and grain boundaries. Each trapping site has a characteristic trapping energy that describes the probability that a trapped atom will be freed again at a given temperature. Higher trapping energies indicate a lower probability of release. The absence of trapping modeling in fuel cycle analysis can be partially justified in designs that use low-Z materials for plasma-facing components (PFC). The main tritium retention mechanisms in low-Z materials is co-deposition with the eroded material from the first wall (FW), with trapping playing a minor role. Several studies showed that C-based or Be-based PFC would have lead to unacceptably high tritium inventory in ITER (i.e. above the regulatory limit, which was originally set to 1 kg [7]) [8–11]. As a result, the focus of PFC development shifted to tungsten. Tritium implantation and trapping are the leading retention mechanisms in high-Z plasma facing materials [9], so understanding these phenomena is crucial to fuel cycle design. Investigations of an ITER wall with all-W PFC, which accounted for tritium trapping and trapping site generation from neutron irradiation, estimated tritium inventories in the range of several hundred grams after approximately 1000 shots [12, 13]. More detailed models projected similar inventories after around 10 000 shots, which was deemed acceptable [14] for ITER. However, this scenario changes significantly for long-term operations in FPPs, which will be subject to higher neutron and ion fluences. Single-component analyses in DEMO blankets suggest that tritium trapping can significantly impact tritium retention in those components, increasing tritium inventories by orders of magnitude ($10^2 - 10^4$) depending on the neutron fluence, materials, and operating temperature [15–17]. At some critical value of trapping probability in PFCs, it becomes impossible to achieve tritium self-sufficiency in an FPP [18, 19]. Therefore, a comprehensive assessment of tritium self-sufficiency must include trapping effects in fuel cycle models.

Updated fuel cycle models must account for several factors. First, radiation damage from the plasma particle and neutron fluxes will create trapping sites in PFCs, vacuum vessel (VV), and blanket structural materials. The evolution of these trapping sites is a complex and non-linear phenomenon that depends on annealing processes, defect dynamics, interactions with gaseous species, and the temporal evolution of the particle flux [20, 21]. The generation of trapping sites amplifies tritium retention and delays the dynamics of the outer fuel cycle (OFC) [3, 4], making tritium self-sufficiency harder to attain.

Second, it is expected that it will be difficult to recover tritium retained in high-energy traps via processes like baking. Ion and neutron irradiation produce high-energy traps, with energies above 1–1.5 eV [22, 23]. Damage-induced traps in tungsten, for example, exhibit a detrapping energy exceeding 1 eV. Experimental analyses of hydrogen trapping on various steels have revealed the existence of irreversible trapping sites within a similar range of trap energy (1–2 eV)[3]. The energy value is contingent upon the temperature at which the samples were analyzed [24, 25]. Figure 1 shows an ideal tritium recovery process via heating from two ideal tungsten components with the same surface area but different thicknesses (1 mm and 2 cm thick, representative of a FW and a divertor tile, respectively). The recovery was simulated with FESTIM [26] by considering a slab with a Dirichlet boundary condition $C_{\mathrm{m}} = 0$ on both sides, where C_{m} is the mobile concentration of tritium. The scripts and the results are available at [27]. It is easier to bake out tritium from the thinner component with its higher surface-to-volume ratio. To completely recover the tritium, temperatures higher than 2100 K are required for the 1 mm-thick component, while a >90% recovery can be achieved above 2700 K for the 2 cm-thick component. Standard *in-situ* baking procedures make use of a hot fluid (e.g. water at 600 K) to recover tritium from the first wall and divertor [28, 29]. However, the required temperatures to recover tritium from damaged-induced traps are much higher (figure 1). It is unclear whether these temperatures can be reached in a tritium recovery system and, if so, whether it would be economically viable to do so.

The fraction of tritium that remains post-heating is trapped in high-energy traps. PFCs, which are most susceptible to these traps due to the high rate of radiation damage they sustain, are expected to require periodic replacement. Assuming that the removed PFCs are baked and the recovered tritium

[3] The term *irreversible trapping* is somewhat ambiguous as it depends on the timescale of interest. A trap with an energy level of 0.5 eV may be considered irreversible at room temperature but could become reversible at very high temperatures or when considering years as the reference timescale.

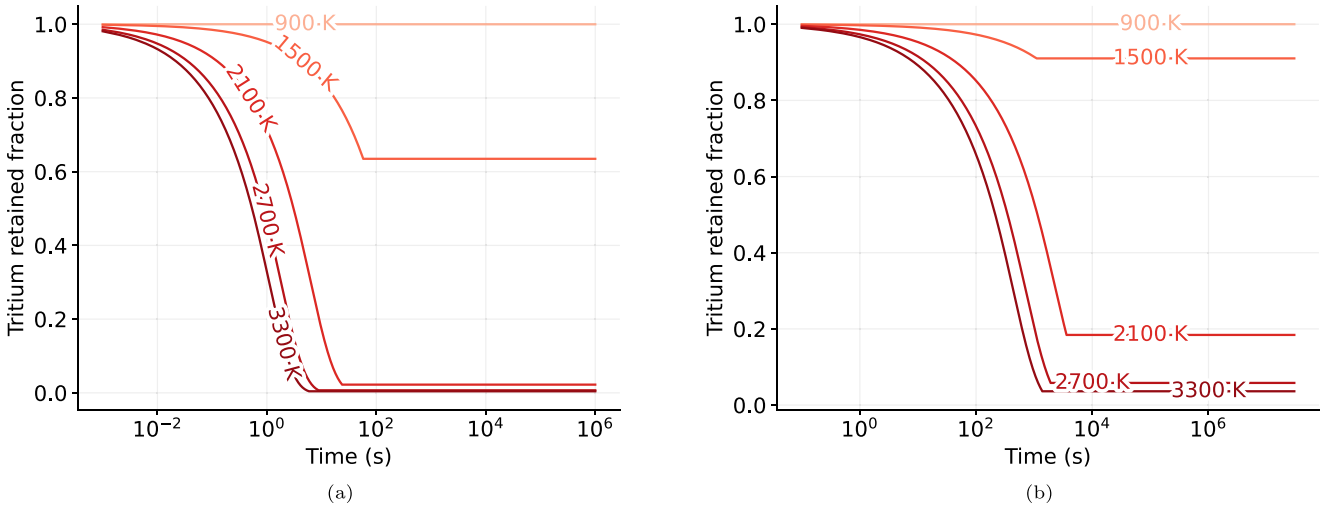

Figure 1. Tritium inventory evolution during recovery from tungsten with damage-induced traps. (*a*) 1 mm thick tungsten component. (*b*) 2 cm thick tungsten component. Tritium recovery by baking is much harder for thick components due to the lower surface-to-volume ratio. For (*a*) most of the tritium can be recovered in less than a hour at $T > 2100$ K. However, ∼20% of tritium is irrecoverable from (*b*) at the same temperature regardless of baking time. Much higher temperatures are required for a complete recovery in a thick component.

reintroduced to the system as fuel, the following factors add to the difficulty of achieving tritium self-sufficiency:

- Permanent loss of unrecoverable tritium in the replaced PFC
- Delayed reintroduction of the recovered tritium to the fuel cycle
- 'Resetting' the saturation of the replaced PFCs

Regarding the third point, tritium trapping eventually saturates on a characteristic timescale that is dependent on component geometry, temperature, and materials. This occurs around 0.23 dpa in W [21][4]. This means that every time a PFC is replaced, there is some time period during which tritium is lost more rapidly from the system due to trapping in the 'fresh' PFC; how this impacts the fuel cycle depends on the the ratio of time-to-replacement and time-to-saturation.

This paper presents a comprehensive approach to incorporating tritium trapping into a dynamic, system-level model of a FPP fuel cycle. It considers both the production of trapping sites due to particle irradiation and the replacement of components. Building upon the model presented in [3], which leverages the residence time method [4, 32], this framework integrates multi-level trapping and trapping sites generation in key components, namely the FW, divertor, and VV materials. The fuel cycle architecture and its operations are modeled using MATLAB Simulink®. Results show that the combined effect of trapping site generation and component replacement heavily affects tritium self-sufficiency, increasing the FPP inventories and setting a higher requirement for the required TBR (TBR_r).

[4] We acknowledge that the interplay between trapping site generation, gas filling of these traps, and defects dynamics might inhibit trap annealing, leading to a situation where saturation is potentially never reached. Advanced experiments that simultaneously investigate material damage and hydrogen exposure at elevated temperatures are necessary to provide insights on this phenomenon, such as those presented in [30, 31].

The paper is structured as follows. Section 2 develops a theoretical, systems-level model for tritium trapping in which trapping is expressed in terms of mobile and trapped inventories. Section 3 presents the results. An ARC-class FPP is considered for the fuel cycle design and operating parameters. However, this analysis can be adapted to any fusion device operating with a D-T fuel cycle. Section 4 frames the results in the context of FPP operations and discusses their implications on long term operations and maintenance, and overall conclusions are presented in section 5. The relevant code, the models and the results are available on GitHub at [27].

2. Methodology

Each fuel cycle component is described by an ordinary differential equation in the form [3, 4]:

$$\frac{\mathrm{d}I_i}{\mathrm{d}t} = \sum_{j\neq i}\left(f_{j\to i}\frac{I_j}{\tau_j}\right) - (1+\epsilon_i)\left(\frac{I_i}{\tau_i}\right) - \lambda I_i + S_i \qquad (1)$$

where we omitted for simplicity the time dependence of the inventories. Subscripts i and j refer to the generic ith and jth component, I is tritium inventory (kg), τ is tritium residence time (s), λ is the tritium decay rate (s^{-1}), ϵ is the fraction of tritium lost due to non-radioactive phenomena (e.g. leakages) (-), and S is a tritium source (kg s^{-1}), and $f_{j\to i}$ is the fraction of tritium flowing from component j to component i.

A detailed description of the model and the ARC-class FPP fuel cycle is provided in [3][5]. We recall that the intermittent nature of the FPP is modeled by using an availability factor AF and a pulse source. The stochastic nature of system failures is not considered explicitly as done in [5], and we used

[5] Note that in this work, the VV structures and the FW are modeled as different components to properly account for tritium trapping in these two components. In [3] they are modeled as a singular component for the ARC-class FPP.

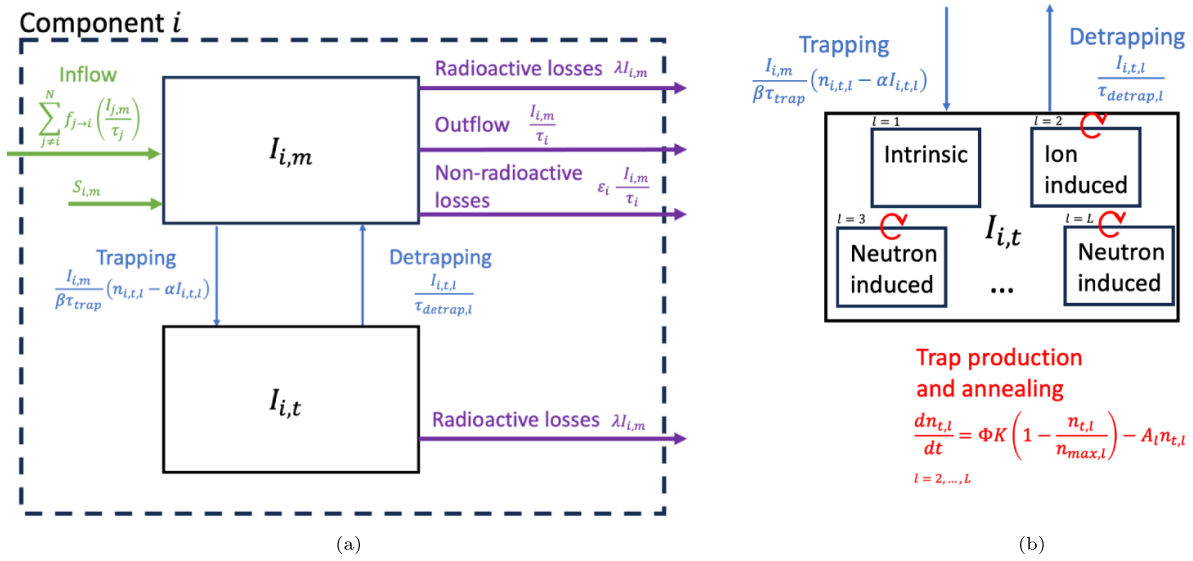

Figure 2. Diagram illustrating the phenomena modeled in this work. (*a*) The tritium inventory of a generic component i, I_i, is divided into mobile inventory ($I_{i,\mathrm{m}}$) and trapped inventory ($I_{i,\mathrm{t}}$). Components connected to each other exchange tritium flows. Tritium is constantly lost due to radioactive decay and non-radioactive losses, such as tritium permeation through component boundaries. Mobile tritium can be trapped, and trapped tritium can be de-trapped. (*b*) Detailed phenomena relevant to the trapped tritium inventory of component i. Intrinsic and damage-induced traps are considered, alongside their production and annealing processes. Traps are produced via neutron and ion irradiation. Produced traps are continuously being created (due to irradiation) and lost (due to annealing), indicated by the red cyclical arrows.

the simplified approach of [4]. We briefly outline key nomenclature essential for this study:

- **Start-up inventory (I_{startup})**. The start-up inventory is the amount of tritium required to start and operate an FPP until it can self-sustain with bred tritium. It is stored in the storage system. Therefore, at the beginning of the operations $I_{\mathrm{storage}}(t=0) = I_{\mathrm{startup}}$.
- **Storage inventory (I_{storage})**. This is the tritium inventory in the FPP's storage system. In the model used here, the storage, management, and delivery system are condensed in a single 'block', reflecting the assumption that all tritium processed and bred within the fuel cycle passes through the storage system. After an initial transient dominated by tritium buildup in fuel cycle-components, the evolution of I_{storage} is dependent on the surplus tritium produced by the breeding blanket [3, 4], but influenced by tritium trapping and component replacement. The storage inventory is of particular interest when analysing fuel cycles because it contains the available tritium to operate an FPP.
- **Reserve inventory (I_{reserve})**. The minimum quantity of tritium in I_{reserve} depends on design, operation, and economic considerations. It exists in addition to I_{storage} to supply backup tritium when needed (e.g. following a tritium loss due to component failures within the fuel cycle). If $I_{\mathrm{reserve}} > 0$ is required at the beginning of the operation, I_{startup} is increased accordingly by I_{reserve}, and $I_{\mathrm{storage}}(t) > I_{\mathrm{reserve}}$ during the initial transient.
- **Mobile (I_{m}) and trapped (I_{t}) inventories**. The mobile inventory accounts for tritium (in any chemical form and present in any medium) that is not trapped at a trapping site. The tritium inventory in a component i is given by the sum of mobile and trapped inventories, i.e. $I_i = I_{i,\mathrm{m}} + I_{i,\mathrm{t}}$.
- **Tritium doubling time (t_{d})**. The tritium doubling time is the time required to double the initial tritium inventory in the FPP, i.e. $I_{\mathrm{storage}}(t = t_{\mathrm{d}}) = 2I_{\mathrm{startup}}$. The definition of t_{d} is not unique [4], and the one used in this work gives the most conservative results in terms of tritium self-sufficiency requirements.

2.1. Tritium trapping and trapping site production

Figure 2 illustrates the source and loss terms for both the trapped and mobile tritium inventories in a generic component i. The model presented here accounts for each of the illustrated terms.

Tritium trapping can be included in the system-level model starting from chemical dilution theory [33]. Equation (2) describes the evolution of the concentration of trapped tritium C_{t} in an arbitrary medium:

$$\frac{\partial C_{\mathrm{t}}(\vec{x},t)}{\partial t} = kC_{\mathrm{m}}(\vec{x},t)\left(n_{\mathrm{t}}(\vec{x},t) - C_{\mathrm{t}}(\vec{x},t)\right) - pC_{\mathrm{t}}(\vec{x},t) \qquad (2)$$

where $C_{\mathrm{m}}(\vec{x},t)$ and $C_{\mathrm{t}}(\vec{x},t)$ are the concentration of the mobile and trapped species (m^{-3}), $n_{\mathrm{t}}(\vec{x},t)$ is the trapping site density (m^{-3}), k ($\mathrm{m}^3\ \mathrm{s}^{-1}$) is a rate constant associated with the trapping process, and p (s^{-1}) is a rate constant associated with the detrapping process.

The first term on the right-hand side (RHS) of equation (2) represents the increase in C_t due to trapping of mobile tritium $C_{\mathrm{m}}(\vec{x},t)$ in available trapping sites (quantified as $n_t(\vec{x},t) - C_{\mathrm{t}}(\vec{x},t)$) at a rate defined by the rate constant k. The second

term on the RHS represents the decrease in C_t due to detrapping of trapped particles $C_t(\vec{x},t)$ at a rate defined by the rate constant p. Equation (2) can be extended to include multi-level trapping (i.e. traps with different trapping energies), as shown in the remainder of this section, and multi-species trapping (e.g. different hydrogen isotopes). However, in this work we consider only multi-level trapping, and defer consideration of multi-species trapping to a future study. Equation (2) cannot be directly implemented in the 0-D fuel cycle model for two reasons [3]. First, the residence time method describes tritium inventories as lumped quantities and not as concentrations, which are a function of space ($\vec{x}$). Second, I_i in equation (1) must be split in two (or more) separate contributions to account for both the mobile and trapped inventories.

Assuming that $n_t(\vec{x},t) - C_t(\vec{x},t)$, p, and k are homogeneous across component i, one can integrate equation (2) over the volume of component i to obtain equation (3):

$$\frac{\mathrm{d}I_{i,\mathrm{t}}(t)}{\mathrm{d}t} = kI_{i,\mathrm{m}}\left(n_{i,t} - \alpha I_{i,\mathrm{t}}\right) - pI_{i,\mathrm{t}} \tag{3}$$

where $I_{i,\mathrm{m}}$ and $I_{i,\mathrm{t}}$ are the mobile and trapped inventory in component i, and $\alpha = \frac{N_A}{10^3 M_\mathrm{T} V_i}$, with N_A Avogadro's number, M_T the molecular weight of tritium (g mol^{-1}), and V_i the volume of component i (m^3) [6].

Equation (3) can be subtracted from equation (1) to obtain suitable expressions for the time dependencies of mobile and trapped tritium in component i:

$$\begin{aligned}\frac{\mathrm{d}I_{i,\mathrm{m}}}{\mathrm{d}t} = &\sum_{j\neq i}\left(f_{j\to i}\frac{I_{j,\mathrm{m}}}{\tau_j}\right) - (1+\epsilon_i)\left(\frac{I_{i,m}}{\tau_i}\right)\\ &- \lambda I_{i,\mathrm{m}} + S_{i,\mathrm{m}} - kI_{i,\mathrm{m}}\left(n_{i,t} - \alpha I_{i,\mathrm{t}}\right) + pI_{i,\mathrm{t}}\end{aligned} \tag{4}$$

$$\frac{\mathrm{d}I_{i,\mathrm{t}}}{\mathrm{d}t} = S_{i,\mathrm{t}} + kI_{i,\mathrm{m}}\left(n_{i,\mathrm{t}} - \alpha I_{i,\mathrm{t}}\right) - pI_{i,\mathrm{t}} - \lambda I_{i,\mathrm{t}}. \tag{5}$$

There are no non-radioactive losses nor streaming terms for the trapped tritium inventory $I_{i,\mathrm{t}}$. A source term $S_{i,\mathrm{t}}$ is included in equation (5) to account for tritium ion implantation that may occur (expected for plasma facing components).

The trapping rate constant k and detrapping rate constant p are:

$$k = k_0 \exp\left(-\frac{E_k}{k_\mathrm{B}T}\right) \tag{6}$$

$$p = p_0 \exp\left(-\frac{E_p}{k_\mathrm{B}T}\right) \tag{7}$$

where k_0 (m^3 s^{-1}) and p_0 (s^{-1}) are pre-exponential factors, E_k and E_p are activation energies (eV), T is the temperature (K), and k_B is the Boltzmann constant (eV K^{-1}).

The diffusion coefficient is expressed as

$$D = D_0 \exp\left(-\frac{E_D}{k_B T}\right) \tag{8}$$

[6] Here, component i is assumed to be a homogeneous medium of material through which tritium moves and is trapped. Real components have complex designs and are often made of multiple materials with different properties. This can be treated explicitly or by lumping parameters.

where D_0 is the pre-exponential factor of the diffusion coefficient [m^2 s^{-1}] and E_D is the activation energy of the diffusion process [eV]. It is usually assumed that E_k, the activation energy for a mobile particle to be trapped, is equivalent to E_D. Considering that diffusion occurs through adjacent interstitial sites at a distance d, k_0 can be expressed as [34]:

$$k_0 = \frac{D_0}{\beta d^2} \tag{9}$$

where D_0 is the pre-exponential factor of the diffusion coefficient (m^2 s^{-1}), β is the interstitial site density (m^3 s^{-1}), and d is the average distance between two interstitial sites (m). For a BCC lattice, $d = \frac{a}{2\sqrt{2}}$, where a is the lattice constant [m].

The detrapping pre-exponential factor p_0 is of the order of 10^{13} s^{-1} [35]. The detrapping energy, E_p, is derived from *ab-initio* calculations or as a fitting parameter from thermal desorption spectroscopy. The latter method is more convenient for our applications as it provides a manageable number of parameters that accurately model macro-scale experiments. It is convenient to define time constants for the trapping (τ_trap) and detrapping (τ_detrap) processes:

$$\tau_\mathrm{trap} = \frac{d^2}{D(T)} \tag{10}$$

$$\tau_\mathrm{detrap} = p^{-1}. \tag{11}$$

Lastly, multiple trap energies need to be accounted for in the fusion materials environment. Defects give rise to distinct trapping sites, each characterized by a different detrapping energy and trap density. Therefore, equations (4) and (5) can be rewritten to include multiple traps:

$$\begin{aligned}\frac{\mathrm{d}I_{i,\mathrm{m}}}{\mathrm{d}t} = &\sum_{j\neq i}\left(f_{j\to i}\frac{I_{j,\mathrm{m}}}{\tau_j}\right) - (1+\epsilon_i)\left(\frac{I_{i,\mathrm{m}}}{\tau_i}\right)\\ &- \lambda I_{i,\mathrm{m}} + S_{i,\mathrm{m}} - \frac{I_{i,\mathrm{m}}}{\beta\tau_\mathrm{trap}}\sum_{l=1}^{L}\left(n_{i,\mathrm{t},l} - \alpha I_{i,\mathrm{t},l}\right)\\ &+ \frac{I_{i,\mathrm{t},l}}{\tau_{\mathrm{detrap},l}}\end{aligned} \tag{12}$$

$$\frac{\mathrm{d}I_{i,\mathrm{t},l}}{\mathrm{d}t} = S_{i,\mathrm{t},l} + \frac{I_{i,\mathrm{m}}}{\beta\tau_\mathrm{trap}}\left(n_{i,\mathrm{t},l} - \alpha I_{i,\mathrm{t},l}\right) - \frac{I_{i,\mathrm{t},l}}{\tau_{\mathrm{detrap},l}} - \lambda I_{i,\mathrm{t},l} \tag{13}$$

where $l = 1, ..., \mathrm{L}$ identifies traps with detrapping energy $E_{p,l}$ and trap density $n_{i,\mathrm{t},l}$. Note that the detrapping frequency is a function of the trapping energy $E_{p,l}$, thus a detrapping time constant $\tau_{\mathrm{detrap},l}$ is associated with each trap. The tritium trapping data used in this work are reported in table 1.

The time evolution of trap density is described by equation (14) [17]:

$$\frac{\mathrm{d}n_{\mathrm{t},l}(t)}{\mathrm{d}t} = \Phi K\left(1 - \frac{n_{\mathrm{t},l}(t)}{n_{\mathrm{max},l}}\right) - A_l n_{\mathrm{t},l}(t) \tag{14}$$

where Φ is the damage rate (dpa s^{-1}), K is the trap creation factor (m^{-3} dpa^{-1}), $n_{\mathrm{max},l}$ is the maximum trap density (m^3 s^{-1}) for trap l, and A_l is the annealing rate (s^{-1}) for trap l. A_l is described by an Arrhenius law, $A = A_0\exp(-E_A/(k_\mathrm{B}T))$.

Table 1. Parameter values used in this work, which updates the residence time method in [3] to include tritium trapping in FW, divertor, and VV components. Three candidate materials are considered for the VV. The pre-exponential factor D_0 for hydrogen diffusion in W [40], Inconel718 [43], and Eurofer97 [48] is divided by $\sqrt{3}$ to account for the $m^{-1/2}$ dependence of the diffusion coefficient of gases [49]. The assumed value for $n_{0,t,1}$ in Inconel 718 and V-4Cr-4Ti corresponds to 10^{-4} at%. We used a_{Fe} [50] for the lattice constant of Eurofer97.

	Material				
Parameters	Tungsten [40–42]	Inconel 718 [43–45]	V-4Cr-4Ti [46, 47]	Eurofer97 [48]	Units
ρ	19.3	8.2	6.1	7.8	$g.cm^{-3}$
ν_0	10^{13}	10^{13}	10^{13}	10^{13}	s^{-1}
$E_{p,1}$	1.0	0.26	0.5 (Assumed)	0.45	eV
$n_{0,t,1}$	2.2	0.88 (Assumed)	0.74 (Assumed)	1.3	$10^{25} m^{-3}$
D_0	$4.1\ 10^{-7}/\sqrt{3}$	$1.07\ 10^{-6}/\sqrt{3}$	$7.5\ 10^{-8}$	$4.57\ 10^{-7}/\sqrt{3}$	$m^2\ s^{-1}$
E_D	0.39	0.51	0.13	0.23	eV
β	6	12	6	6	—
a	316	360	303	286	pm

We acknowledge that the annealing rate will be impacted by defect stabilization mechanisms linked to the presence of hydrogen or any other gas. The relationship between irradiation damage and the presence of hydrogen in the lattice has been investigated theoretically [36] and experimentally [30], showing that the presence of hydrogen isotopes impedes defect annealing, resulting in increased hydrogen retention, especially at low temperatures. Additionally, the data for ion- and neutron-induced traps available in literature [17] (see appendix) might not reflect the full complexity of defect evolution. The physical picture is further complicated by the dose rate at which the material is damaged, which can affect retention. However, these phenomena have yet to be investigated in detail in fusion relevant conditions, and we limit our analysis to the simple trap dynamics described by equation (14).

We assume the ion-induced traps to be localized in a thin layer of the FW ($\sim$2.5 μm) [21], whereas neutron-induced traps are homogeneously distributed through the thickness of the materials. A comparison between the system level model here presented (equations (4) and (5)) and a detailed 1D tritium transport model developed in FESTIM [26] reveals that the 0D system level model accurately captures the evolution of trapped inventories in plasma facing components with a high degree of precision. The only discrepancy observed is a slight overestimation of tritium ion implantation from the plasma source by the system-level model. However, the contribution of ion-induced traps is negligible compared to neutron-induced traps, and the inventories are dominated by tritium trapped in neutron-induced traps (section 3). The comparison between the two models is available as additional material in the GitHub repository [27].

The initial condition for the trap density is given by $n_{t,l}(0) = n_{0,t,l}$, which is equivalent to the number of intrinsic traps. The maximum number of intrinsic traps in a component is at its maximum at $t = 0$, whereas there are no ion- or neutron-generated traps at $t = 0$. For this study, the FW tiles and divertors are assumed to be made of tungsten. Three candidate materials (Inconel 718, V-4Cr-4Ti alloy, Eurofer97) are considered for the VV and blanket structures.

No data is available for neutron-induced traps in structural materials. Compared to W, Eurofer97 exhibits lower hydrogen retention by a factor of $\sim$6 when damaged with W ions at 300 K [37]. There are no comparisons available for hydrogen retention behavior between W and Ni-based alloys (e.g. Inconel 718). Ni-based alloys are more susceptible to void formation and growth due to (n,α) and (n,p) reactions with Ni-59 at thermal neutron energies. The average void size and the size of the largest voids are much higher in neutron-irradiated Ni-based alloys than in irradiated W at similar doses (<25 nm average and 100 nm for large voids in Ni-based alloys [38] versus 4-7 nm average and 13 nm for large voids in W [31]). This suggests that hydrogen retention in damaged Inconel 718 may be higher than in damaged W. Concerning V-alloys, D-irradiated V-4Cr-4Ti exhibits higher hydrogen retention than W at 380 K and 573 K, but the retention becomes comparable at 773 K [39], which is close to the operating temperature of a liquid immersion blanket.

In the following analysis, we assume that the neutron-induced trap density and energy in structural materials are the same as in W. Based on the previous considerations, the results might be realistic for V-4Cr-4Ti alloy, overestimated for Eurofer97, and underestimated for Inconel 718.

2.2. Component replacement

Due to very harsh operating conditions, it is anticipated that many FPP components will require regular replacement. Maintenance strategies have been proposed to address the replacement of divertors, FW tiles, blanket modules, and VV [51–55]. The replacement time for each component is uncertain, although we may expect a lifetime of 1–10 years for the components that are most relevant to this analysis (e.g. in-vessel components that are expected to trap the most tritium)[7]. The mobile tritium inventory might be recovered before replacement, while trapped tritium (especially if trapped in

[7] The mean time between failures may be much lower for first-of-a-kind components, as noted by [4]. However, the consequent low availability due to frequent replacements could also hinder the FPP from achieving tritium self-sufficiency, underscoring the importance of designing the fuel cycle with a holistic view that accounts for maintenance and operations planning [3, 4].

Table 2. Replacement times and volumes of FW (first wall), divertor, and VV (vacuum vessel) assumed in this work for an ARC-class FPP. Divertor and FW volumes are taken from a detailed CAD model of an ARC-class tokamak [56] that does not necessarily reflect an updated commercial design.

Parameter	Symbol	Value	Units
VV replacement time	$t_{\mathrm{repl,VV}}$	2	y
Divertor replacement time	$t_{\mathrm{repl,div}}$	2	y
FW replacement time	$t_{\mathrm{repl,FW}}$	2	y
VV volume	V_{VV}	3.5	m^3
Divertor volume	V_{div}	0.17	m^3
FW volume	V_{FW}	0.17	m^3

high energy traps) is hard to recover unless destructive techniques are used to increase the surface-to-volume ratio of the component (see also figure 1). We conservatively assume that trapped tritium is not recovered, and we discuss this assumption in section 4.1.

The replacement is implemented in the Simulink® model by exploiting a clock block that resets the trapped inventory when the component is replaced. The downtime due to maintenance activities is still averaged over one year based on the assumed availability factor, as was done in [3]. The data used to model component replacement is reported in table 2.

3. Results

To best understand how tritium trapping impacts the fuel cycle, we organize the results by progressively introducing more complex, realistic scenarios. Initially, we consider only intrinsic traps in undamaged materials. Next, we consider tritium trapping at radiation-induced defect sites (section 3.1). Finally, we explore the influence of component replacements (section 3.2) by accounting for both trapping population evolution in the new component and device downtime required for maintenance. Lastly, in section 3.3 we conduct a sensitivity analysis on the ion flux fraction impinging on the FW and divertor and on material temperature. These two parameters are crucial to the accurate description of tritium trapping. The outcomes from this section are summarized in terms of variations in $\mathrm{TBR_r}$ and I_{startup}.

Figure 3 shows the baseline case for an ARC-class FPP ($\mathrm{TBR_r} = 1.07$ and $I_{\mathrm{startup}} = 1.45$ kg) without trapping. Input parameters for this model are reported in [3]. Figure 3 shows small deviations from the results reported in [3] due to the use here of a numerical solver with higher tolerance of the numerical solver and different timesteps. This was necessary to resolve the effects of trapping and be consistent with the significant digits of tritium trapping properties. The FPP subsystems with the largest tritium inventories are shown. These are the tritium storage system (> 1 kg), the isotope separation system with ∼260 g of tritium, the tritium extraction system with ∼60 g of tritium, and the breeding zone with ∼3.5 g of tritium. The tritium inventory in the FW and divertor is negligible at ∼1 mg.

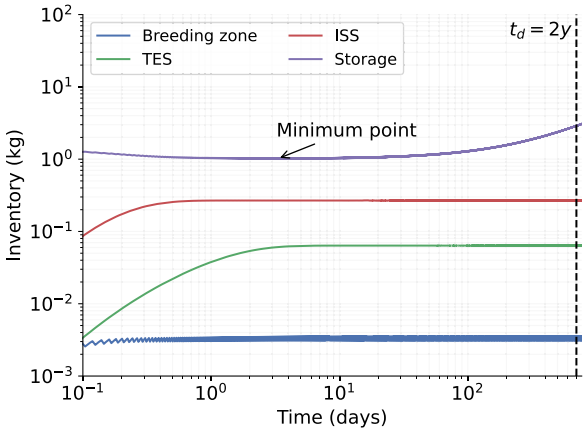

Figure 3. Evolution of relevant tritium inventories for the baseline (no traps) case. A $\mathrm{TBR_r} = 1.07$ is required to meet the target doubling time, $t_{\mathrm{d}} = 2$ y. FW and divertor inventories are not shown because out of scale (∼1 mg).

Figure 4 shows the key results from this analysis. The evolution of the storage inventory is plotted for the baseline (no traps) in figure 4(*a*). Figure 4(*b*) shows how intrinsic traps in the material affect storage inventory evolution. Figure 4(*c*) repeats the analysis but considers damage-induced traps as well. Figure 4(*d*) adds in consideration of component replacement. The target doubling time is kept fixed at $t_{\mathrm{d}} = 2y$. Comparison of figures 4(*a*) and (b) shows that intrinsic traps alone are not expected to change fuel cycle dynamics, and $\mathrm{TBR_r}$ and I_{startup} remain effectively the same as in the baseline case. However, damage-induced traps have a significant impact on the fuel cycle. This is evident in the sharp increase of $\mathrm{TBR_r}$ and I_{startup} in figure 4(*c*), which is needed to maintain the fixed doubling time (2 y). Including component replacements for the FW, divertor and VV (figure 4(*d*)) further increases $\mathrm{TBR_r}$, while I_{startup} remains unaltered because the initial transient is unaffected by the replacement, which takes place after 1.7 y in this specific case. We chose to model component replacement at $t = 1.7$ y due to the fixed doubling time of two years, preventing us from observing the effects of replacement at $t = 2y$. Given that the trapped tritium population reaches steady state in much less than a year, the replacement could have been executed at any time $1 < t < 2y$ with identical outcomes.

Figure 5 shows the storage inventory dynamics when $\mathrm{TBR_r}$ and I_{startup} are kept fixed at their baseline case values and t_{d} is allowed to vary. Figure 5(*d*) shows the combined effect of trapping and component replacement in this case. It shows that the impact on available tritium reserve in the event of a fuel cycle failure is significant: failure to account for tritium trapping results in overprediction of available storage inventory by about 1 kg. The effects of tritium trapping also force an increase in t_{d} when $\mathrm{TBR_r}$ and I_{startup} are held fixed. Accounting for trapping and component replacement increases t_{d} from 2 y

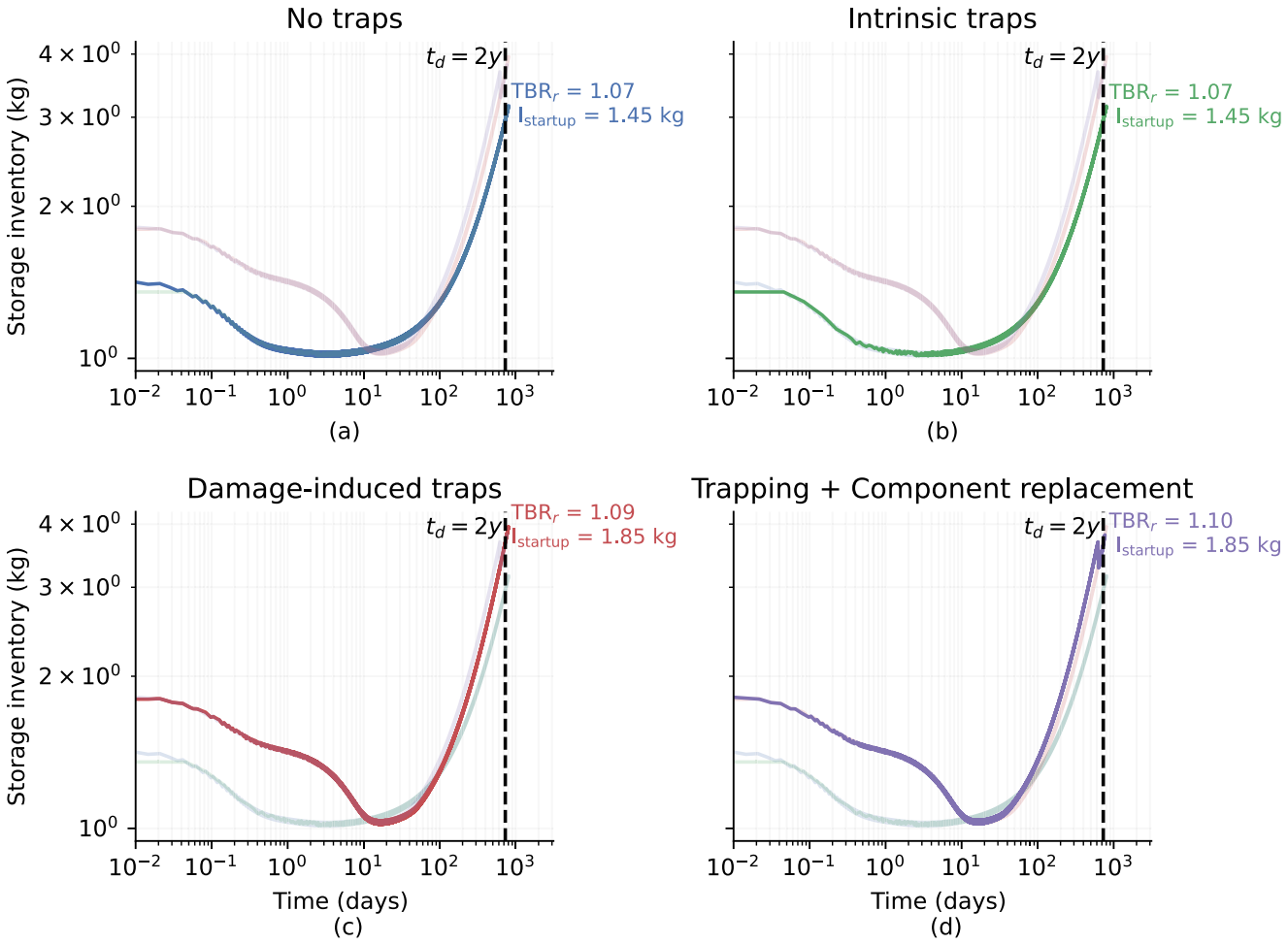

Figure 4. Storage inventory evolution at fixed doubling time ($t_d = 2\,y$) for (*a*): no traps; (*b*): intrinsic traps only; (*c*): trapping site generation; (*d*): trapping site generation and component replacements. The corresponding curve is highlighted in each panel. The key metrics for each scenario (TBR_r and $I_{startup}$) are listed. Intrinsic traps have no discernible impact on tritium storage inventory evolution. A large increase in TBR_r is observed when accounting for damage-induced traps and component replacements for the first wall, divertor, and vacuum vessel. Note the log scale on the time axis to highlight the initial transient.

to 3 y. These results are discussed in detail in the following subsections.

3.1. Impact of trapping on tritium self-sufficiency

3.1.1. Trapping in undamaged materials. The negligible impact of intrinsic traps in undamaged materials ($n_{0,t} \approx 10^{-4}$ at%) on tritium self-sufficiency and tritium inventories is illustrated in figure 4(*b*). The TBR_r remains unaltered compared to the baseline case. This can be explained by computing the steady-state trapped tritium inventory (in intrinsic traps, i.e. $l = 1$) from equation (13) by setting the time derivative and the source term equal to zero:

$$I_{i,t,1} = \frac{1}{\frac{\beta\tau_{trap}}{\tau_{detrap} I_{i,m}} + \frac{\beta\lambda\tau_{trap}}{I_{i,m}} + \alpha} n_{0,t,1} \tag{15}$$

which results in a negligible amount of trapped tritium ($I_{FW,t} \sim I_{div,t} \sim 0.1$ mg and $I_{BZ,t} \sim 0.7$ g). This is because the mobile tritium inventory in the FW, divertor, and blanket is low ($I_{FW,m} \sim I_{div,m} \sim 1$ mg and $I_{BZ,m} \sim 3$ g).

3.1.2. Trapping site generation in damaged materials. The first wall, divertor, and structural materials will be damaged at a high rate (∼20 dpa/FPY [52]) in an FPP. While tungsten is well characterized with regards to damage-induced traps [14, 21], the structural materials are not. As we do not have trapping density data for Eurofer 97, Inconel 718, or V-4Cr-4Ti, we used trapping density and energy data for tungsten to model the VV's behavior. No ion-induced traps are present in the structural materials because they are not exposed to the plasma ion flux. Trap generation and filling takes a long time compared to the fuel cycle dynamics (days vs hours) (figures 4(*c*) and 5(c)). The storage inventory minimum occurs at ∼30 days when accounting for trap generation due to radiation damage, compared to ∼3 days for the baseline (no trapping) case. Since the traps are a tritium sink, higher TBR_r and $I_{startup}$ are required to achieve tritium self-sufficiency. The tritium loss associated with the damage-induced traps amounts to ∼35 g in the FW and in the divertor (a ∼3500× increase compared to the baseline case) and 440 g in the VV (a ∼150× increase compared to the baseline case). The results are consistent with the increase in tritium inventory predicted with

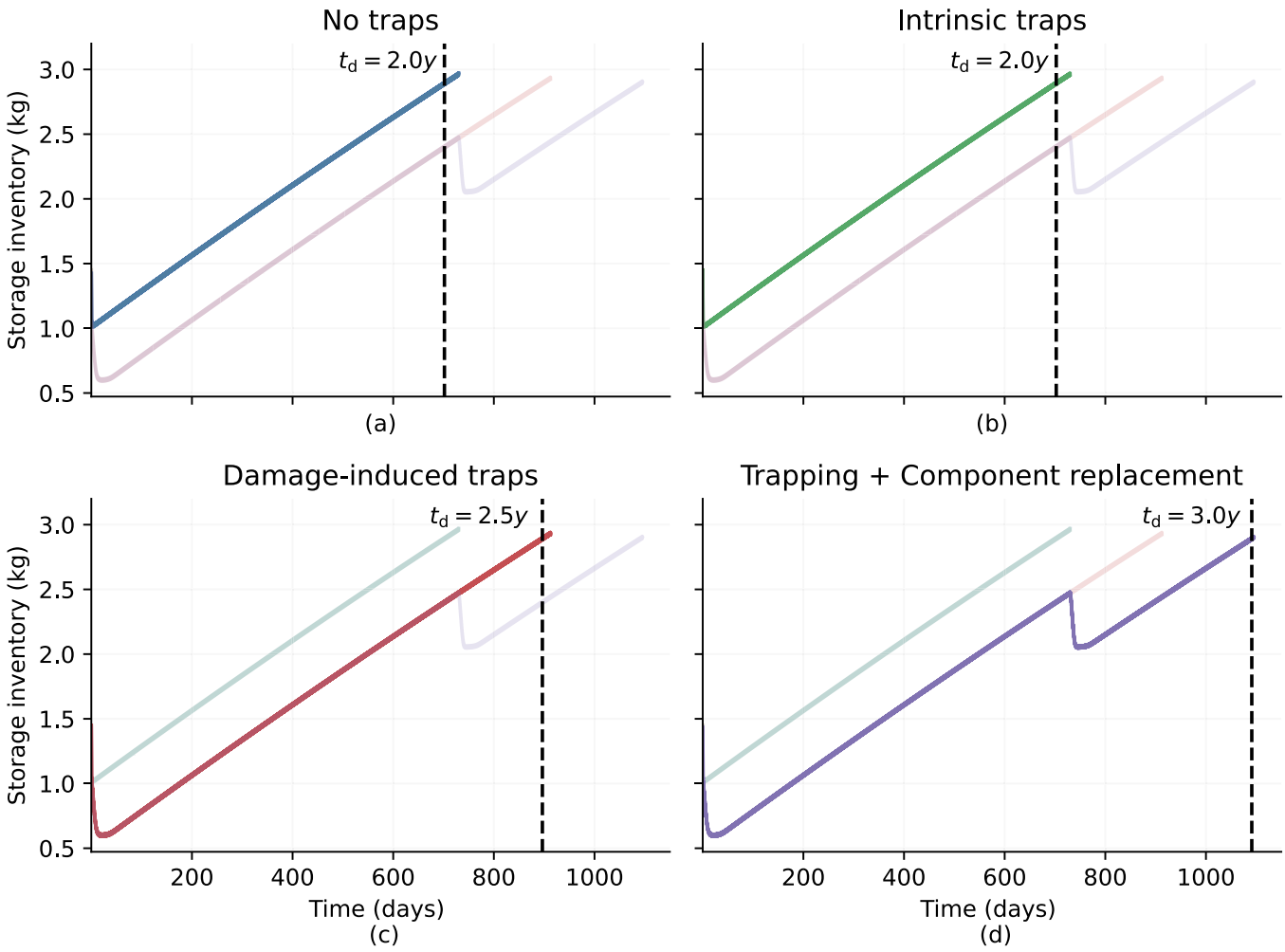

Figure 5. Storage inventory evolution for $\mathrm{TBR_r} = 1.07$ and $I_{\mathrm{startup}} = 1.45$ kg (kept fixed at the values of the baseline case) for (*a*): no traps; (*b*): intrinsic traps only; (*c*): trapping site generation; (*d*): trapping + component replacements. No significant differences appear between the case with no traps and intrinsic traps only because of the very small impact of intrinsic traps. An increase in the doubling time is observed when damage-induced traps are considered. Component replacements further increase the doubling time. Note the linear scale instead of the log scale as in figure 4 to highlight the increase in doubling time.

a component-level model of tritium trapping in tungsten at 1000 K at 20 dpa/FPY [17].

Trap generation has a significant impact on tritium self-sufficiency. In order to account for this, FPP designers will likely need to accept longer doubling times (which has important implications for fusion power expansion) or design blankets that can achieve higher TBRs while also accepting a higher required startup inventory (which presents notable engineering and regulatory challenges). Furthermore, trapped tritium contributes significantly to the specific activity of the VV. The specific activity due to tritium amounts to 10^{13} Bq kg^{-1} after 2 y of irradiation assuming 70% availability. This value is comparable to the total specific activity (10^{14} Bq kg^{-1}, falling below 10^{13} Bq kg^{-1} within a year) computed for a V-Cr-Ti vacuum vessel after 2 years operation in a comparable power plant [57]. Total activity depends on the VV material and radiation exposure, but if using low-activation materials, trapped tritium dominates overall radioactivity on short timescales. Trapped tritium must be accounted for when designing maintenance schemes. Frequently replaced components are likely to contain significant amounts of trapped tritium, which impacts safety and handling.

3.2. Impact of component replacement on tritium self-sufficiency

While trapping sites eventually saturate, component replacement introduces a 'fresh' tritium sink in the fuel cycle. We assumed that the mobile inventory is recovered from the removed component via processes like baking, and only the trapped inventory is lost. Figure 6 illustrates the inventory evolution assuming replacement of the VV, FW, and divertor every 2 years. The replaced components behave like a tritium sink until the trapping sites saturate again. The storage inventory drops accordingly to balance the additional tritium needed. The impact of the replacement is substantial and increases the doubling time to $t_d = 3$ y at fixed $\mathrm{TBR_r}$. If $t_d = 2$ y is a firm requirement, TBR in the breeding blanket must increase from

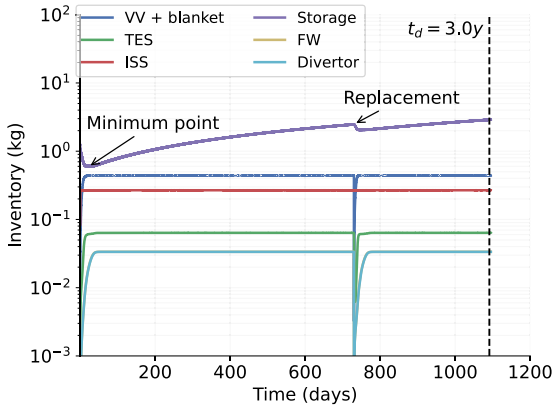

Figure 6. Evolution of relevant tritium inventories for $TBR_r = 1.07$ and $I_{startup} = 1.45\,kg$ (baseline case) considering trapping (intrinsic and extrinsic), and component replacement. The doubling time is significantly increased because of the component replacement (VV, FW, and divertor). First wall and divertor curves overlap.

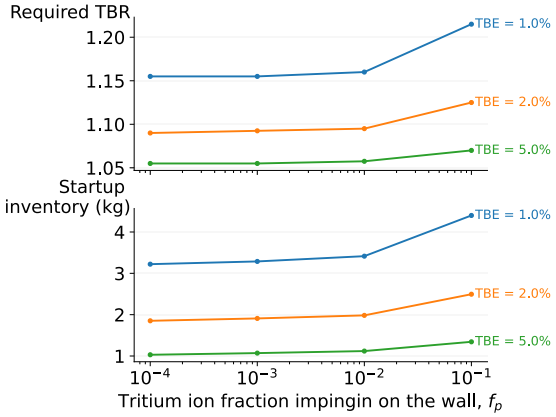

Figure 7. TBR_r and $I_{startup}$ for different values of tritium ion flux impinging on the FW and divertor, considering trapping. Tritium self-sufficiency is weakly affected for $f_p < 10^{-2}$, while the impact becomes significant at $f_p > 10^{-2}$.

1.07 to 1.10, which must be accounted for early in the design stage of the FPP. The start-up inventory is not affected because the replacement takes place much later than the initial transient (until the minimum $I_{storage}$ is reached), which has been shown to drive the requirements for $I_{startup}$ [3].

A comparison of figure 6 with figure 3 shows that accounting for tritium trapping and component replacement significantly changes the tritium inventory evolution of the FPP. The inventory in the VV dominates in this case (440 g), and the FW and divertor inventories increased up to ∼35 g.

3.3. Sensitivity analysis

3.3.1. Ion flux to the first wall and divertor. The baseline scenario considered in the previous sections assumed that a fraction of tritium ions injected into the plasma impinge on the FW and divertor ($f_p = 10^{-4}$) [3]. The results indicated that tritium trapping in PFCs is negligible if considering only intrinsic traps (section 3.1.1), while its contribution (∼35 g) becomes comparable to other relevant inventories (e.g. ∼60 g in the TES) when accounting for damage-induced traps. The impact on tritium self-sufficiency remains mostly constant regardless of the tritium burn efficiency (TBE [58]) for $f_p < 10^{-2}$, as illustrated in figure 7. Beyond this threshold, f_p dramatically impacts tritium self sufficiency. This is caused by dual effects: increased tritium implantation into PFCs and a reduced tritium exhaust from the divertor pumps. For instance, at $f_p = 0.1$, the tritium flow rate in the inner fuel cycle decreases by 10% compared to the baseline case. Simultaneously, tritium implanted in PFCs experiences a longer residence time in the OFC before reaching the storage system. At low TBE (TBE = 1%) the impact is extremely high, with a 5% increase in TBR_r and 30% increase in $I_{startup}$ when increasing f_p from 10^{-4} to 10^{-1}. Compared to the baseline case (TBE = 2%), TBR_r increases from 1.09 to 1.13 and $I_{startup}$ from 1.85 kg to 2.50 kg. For higher values of TBE the impact of f_p is weaker but still relevant.

3.3.2. Temperature. In our model, the operating temperature affects hydrogen diffusion coefficients, trapping rates, and detrapping rates, which all follow an Arrhenius law. A parametric scan over the range 500 –1000 K was performed to assess the impact of tritium trapping at different operating temperatures in the blanket[8], FW, and divertor. The 500 –700 K temperature range can be considered representative of water-cooled and helium-cooled lithium lead blankets featuring Eurofer 97 as structural material [59–61], while 800 –1000 K is the expected range for FLiBe liquid immersion blankets exploiting high temperature alloys such as Inconel or V-Cr-Ti alloys [52, 56, 62, 63]. Liquid lithium blankets are expected to operate somewhere in the middle of this range, although Li blanket designs are not available in literature for reference. The analysis was performed over the 500 –1000 K range for each structural material considered, although we acknowledge that in practice the operating temperature window may be more constrained (e.g. the Eurofer97 maximum operating temperature is 800–900 K [64]). Results are shown in figure 8. TBR_r and $I_{startup}$ are strongly impacted by operating temperature: higher operating temperatures relax requirements on TBR_r and $I_{startup}$. At lower temperatures, TBR_r may be hard to achieve in the current breeding blanket designs. Recent studies show maximum achievable TBRs in the 1.15-1.20 range, but only for highly optimized, simplified blanket models (e.g. ARC-class tokamaks [65, 66]; and various DEMO blanket concepts [67–69]). Similarly, $I_{startup}$ is much higher at lower operating temperatures. At 500 K, the FW and divertor inventories reach ∼135 g, while the VV/blanket retains ∼1.5 – 1.8 kg of tritium depending on the material. As the temperature increases, the impact of tritium trapping on TBR_r and $I_{startup}$ decreases. In general, operating at higher temperatures may be an effective strategy to counteract tritium retention in components because it increases the detrapping rate and

[8] In the ARC-class tokamak, the blanket and VV are considered as one component for this part of the analysis.

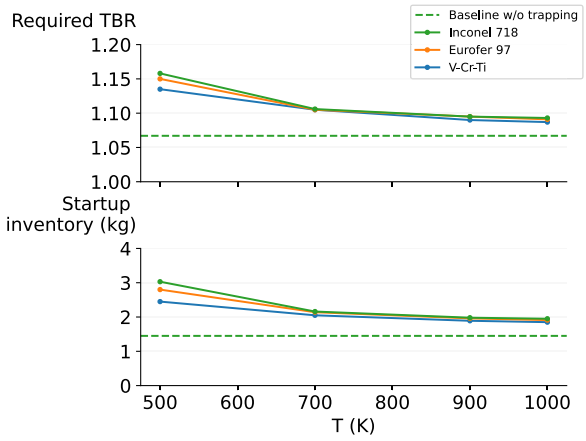

Figure 8. TBR_r and $I_{startup}$ for different values of of materials temperature, considering trapping in FW, divertor, and VV. Tritium self-sufficiency is strongly affected by the temperature of these components.

reduces defect stabilization. This has been observed experimentally; for instance, full recovery of damage-induced traps was recently observed in Eurofer 97 at 620 K [70], suggesting that operating at medium-to-high temperatures would be beneficial. However, defect formation mechanisms, such as those described in [31, 71, 72], may become predominant at very high temperatures, leading to the opposite effect (increased retention).

As a speculative exercise, we conducted a tritium self-sufficiency analysis for a very-high-temperature scenario, assuming a twofold increase in tritium retention in the FW, divertor, and VV. This scenario raises the required TBR to $TBR_r = 1.11$ and the start-up inventory to $I_{startup} = 2.16$ kg. These values should not be interpreted as upper bounds, as no saturation was observed up to 2.3 dpa [73], and inventories and TBR_r would likely increase at higher fluences. Ideally, data would be obtained indicating if and when trapping saturates as a function of dpa, and this data would be used to repeat the full analysis presented in this paper.

4. Discussion

This study underscores critical research needs related to tritium trapping in fuel cycles. It is necessary to accurately characterize defect populations in structural materials exposed to fusion neutron irradiation, as defects act as trapping sites. In the absence of a high-flux fusion neutron source, advanced computational studies of materials damage will be important. Tritium trapping will impact tritium self-sufficiency, so a better understanding is needed to design effective fuel cycles. Achieving tritium self-sufficiency will be challenging, assuming that tungsten's behavior is a good proxy for how radiation damage will evolve in structural materials. In addition to the issue of tritium loss from the fuel cycle due to trapping, the associated buildup of tritium inventory in structural materials (10 s to 100 s of grams) presents safety and regulatory challenge (section 3.1.2). Fuel cycle and blanket models that do not account for trapping may overestimate the plant's ability to achieve tritium self-sufficiency.

4.1. Maintenance

Maintenance strategies in a FPP could be profoundly impacted by tritium trapping. Our findings indicate that trapped tritium contributes to the specific activity of the FW, divertor, and structural materials by an amount comparable to the activity resulting from neutron activation products in the same components [57]. Remote handling procedures will already be in place for in-vessel component replacement due to high levels of neutron activation, but tritium content may require additional safety measures. While tritium contribution to the contact dose rate is negligible due to the short penetration depth of β radiation from tritium decay, its high mobility during handling procedures can lead to contamination of rooms and instrumentation. Tritium recovery will be required prior to component disposal, or a venting and detritiation system will be needed, as otherwise tritium might easily diffuse through the component and be released in the rooms. Most tritium removal techniques explored in the literature focus on carbon PFC, where co-deposition is the main retention mechanism [9, 74, 75]. However, these techniques are not effective at removing tritium trapped in the bulk material. Isotopic exchange was shown to be effective at removing tritium from the surface of tungsten components, but the process is very slow for bulk tritium removal [76]. A potential solution for removing tritium trapped in the bulk material is high-temperature baking. However, this process is effective only at very high temperatures for tritium in high energy traps (see figure 1), but high temperature baking (or melting) is energy-intensive and could be cost-prohibitive.

Scheduled maintenance must be carefully planned. This analysis shows that tritium self-sufficiency is strongly influenced by tritium trapping dynamics, which is in turn affected by component replacement. If there is a large amount of trapping, and the retention time scale is fast in the replaced component relative to inventory doubling time, then component replacement can significantly affect the plant's ability to achieve tritium self-sufficiency. On the other hand, if the retention time scale is slow compared to inventory doubling time, then component replacement may have only a minor impact on TBR_r . Prioritizing the replacement of components with a large trapped inventory during scheduled downtimes proves advantageous.

4.2. Start-up inventory and reserve inventory

Since the reserve inventory accounts for a large fraction of the start-up inventory, its optimization is advisable. The reserve inventory plays a crucial role in the period after startup, when the storage inventory has not yet begun steadily increasing, necessitating the availability of a backup tritium source that can be used to ensure continuous operation in the event of a partial fuel cycle failure [3, 4]. Figure 4 shows that accounting for damage-induced traps impacts the storage inventory

evolution significantly and lengthens its initial transient behavior, such that it reaches its minimum in ∼20 days instead of 1–2 days. This therefore has clear implications for the reserve inventory. The reserve time t_{res} is the amount of time that the FPP can operate using tritium from the reserve inventory $I_{reserve}$. It is typically assumed that t_{res} is comparable to the time of the initial transient, which lasts from the start of operation to the time when $I_{startup}$ reaches a minimum. For example, in the baseline cases described in [3, 4], $t_{res} = 24$ h and the initial transient lasts 2–3 days. By accounting for tritium trapping, the initial transient period increases by ∼10×, to about one month long (section 3.1.2). The corresponding increase in $I_{reserve}$ could be prohibitive for large scale FPPs. Therefore, an optimization of $I_{reserve}$ is needed that accounts for the probability of failure during the initial transient and sets t_{res} accordingly.

4.3. Operating temperature

Lower operating temperatures (500–700 K) results in increased trapping (figure 8), increasing $I_{startup}$ by 50% and increasing the trapped inventory in the FW, divertor, VV, and blanket relative to high temperature ($>$ 900 K) operation. Taking the ARC-class FPP modeled in this work as an example, the tritium inventory in the FW and VV (assumed to be made of V-4Cr-4Ti) are 135 g and 1.5 kg respectively at 500 K. At 1000 K, the inventories drop to 35 g and 0.44 kg (section 3.3.2).

Higher temperature operation improves the thermodynamic efficiency of FPPs and decreases tritium trapping. As maximum operating temperatures are constrained by the operating limits of components and materials, these results further demonstrate that the development of advanced fusion materials for high-temperature service should be a key research priority.

However, very high operating temperatures could also lead to the formation of complex defect structures that increase tritium retention. Therefore, an optimal operating temperature might exist at a point where annealing dominates defect evolution and happens at a sufficiently high rate that the formation of large, tritium-trapping voids is precluded [73].

4.4. Plasma-material interactions

The current study considers some of the effects of plasma-material interactions on the fuel cycle, such as ion-induced traps and ion implantation. However, the model presented here does not account for all phenomena. For example, the interplay between ion implantation flux and radiation damage evolution in FW materials has not been well characterized. Trapped hydrogen in the FW may greatly reduce annealing, leading to a significant increase in the trapped tritium inventory. In fact, [30] showed that W samples exposed to simultaneous W and D irradiation had increased tritium retention relative to W samples subjected to the same two irradiations in sequence. The presence of D ions during exposure stabilizes the radiation defects, leading to much stronger tritium retention at low temperatures (300 K). This effect decreases with temperature due to the higher de-trapping rate of D, which reduces defect stabilization and decreases the number of trapping sites [77].

Additionally, the chemical bonding of tritium ions on the surface of the walls has been neglected in this model. Wall conditioning via addition of a thin layer of low-Z material (e.g. Li or B) is a common practice to limit sputtering of the high-Z FW material. While this practice is effective in reducing core plasma contamination due to high-Z impurities, the low-Z material layer can form strong chemical bonds with hydrogen, resulting in an additional tritium sink.

The co-deposition of tritium with eroded material is also neglected. Modeling the effects of this phenomenon entails two challenges: quantifying the amount of wall material that is eroded, and quantifying the amount of tritium that co-deposits with it. Although trapping is the primary retention mechanism of tritium in W, co-deposition acts as an additional tritium sink.

Lastly, the fraction of tritium ions impinging on the walls has been shown to strongly affect tritium self-sufficiency above a certain threshold (section 3.3.1). This underscores the importance of quantifying f_p from experiments or from plasma physics simulations. From a plasma operation perspective, schemes that utilize plasma turbulence to increase the scrape-off layer width may likely increase the ion flux to the wall. Therefore, a trade-off might arise between heat flux management at the divertor and limiting tritium implantation in the FW.

4.5. Advantages and limitations of the model

The tritium trapping model presented in section 2 offers several key advantages over the simplified, physics-agnostic approaches used in previous fuel cycle models [4–6, 32]. Approaches such as using a user-defined fraction of tritium retained in a component, or incorporating a sink term that saturates at a predefined value, rely heavily on external data from component-level models or experiments. These data must align closely with the operating conditions of the fuel cycle model, which poses significant limitations. Experimental data are typically based on conditions relevant to experimental devices rather than those of an FPP, and they cover a narrow set of materials and operating temperatures. Furthermore, running component-level models for every relevant set of inputs would not only be computationally intensive but also fail to account for the dynamic interactions among different components in the fuel cycle. In contrast, the physics-based trapping model implemented in this work eliminates these constraints. By explicitly modeling tritium trapping and material damage dynamics, the model can account for any material or operating temperature, provided the necessary properties are known. This approach enables more realistic estimations of trapped inventories and ease the exploration of the design space. Regarding the limitations of the trapping model presented in this work, it adopts the same approach as previous studies on hydrogen retention in fusion components [34, 78–80]. The main underlying assumption is that tritium transport can be described at a macroscopic level using the parameters (p, k, D, A) and a few trapping energies representative of the energy

landscape of the material. This approach is usually satisfactory (e.g. the models used in [34, 78–80] were validated against experiments), but the complexity of irradiation damage might introduce phenomena for which the model does not account.

For instance, the conventional point defect model of tritium transport assumes that each trap can accommodate a fixed amount of hydrogen (in our model, a single atom). However, detailed cavity descriptions using a non-equilibrium thermodynamic model showed that the point defect model may not accurately describe the amount of hydrogen that can be trapped in voids [71, 72]. Large amounts of tritium trapping in voids has been observed in fission-neutron-irradiated tungsten [31]. Recent research (unpublished at the time of this work) found that at high temperatures (∼1350 K), tritium retention and the tritium saturation concentration increased [73]. The density and size of defects in W were very similar to those described by [31], suggesting that the transition from vacancies and small vacancy clusters to large voids leads to an increase of tritium retention consistent with the cavity descriptions of [71, 72].

Note that the data for neutron-damage-induced traps in tungsten are derived from self-ion irradiation experiments [37, 81–83, 84]. Heavy ion irradiation has been shown to be a reasonable proxy for neutron damage. W samples irradiated in the High Flux Isotopic Reactor [20] exhibited radiation defects comparable to the defects observed in self-ion irradiated W [85] at low dpa (<0.3) and room temperature[9] Due to the absence of a high-energy, high-fluence neutron source that could provide more reliable data, these values are considered acceptable to describe neutron-induced traps and perform tritium retention analyses [42, 79]. However, the effect of fusion neutrons (i.e. 14 MeV neutrons) might not be exactly replicated by self-irradiation experiments. Similarly, we assumed the neutron-induced trap energy and density in structural materials to be the same as in W, considering that the FW and the VV are two adjacient components in ARC-class tokamaks, thus experiencing similar neutron fluence at comparable energies. These assumptions highlight the crucial needs for reliable data on trap energy, trap density, and defect evolution in neutron-irradiated structural materials.

5. Conclusions

Tritium trapping must be considered when assessing tritium self-sufficiency and tritium inventories in FPP. This study represents a step forward in explicitly accounting for tritium trapping through a physics-based model within a dynamic, system-level framework to quantify fuel cycle requirements. Intrinsic traps in FW, divertor and VV materials do not significantly impact tritium self-sufficiency, while damage-induced traps lead to a 2.5% increase in the required TBR and a 30% increase in the required start-up inventory. We emphasize that 2.5% is a nontrivial increase in the required TBR, considering the difficulty of achieving a high TBR in state-of-the-art blanket designs. It would be very difficult to add breeder or multiplier volume to achieve an extra 2.5% increase in TBR in a near-final FPP design, so trapping effects must be accounted for early in the design stage. Furthermore, if a large fraction (f_p) of tritium ions are trapped in the FW and divertor materials, the increase in the required TBR can be as high as 5%. Component replacements further complicate tritium self-sufficiency by introducing a large, periodic tritium sink in FPP operations. Beyond the implications for tritium self-sufficiency, the combination of tritium trapping and component replacements imposes burdens on maintenance and waste disposal. Tritium inventories trapped in replaceable components are in the range of ∼10 g—100 g, necessitating stringent radiation protection procedures and requiring detailed safety analysis to assess whether these inventories might be mobilized in the event of an accident. Lastly, the periodic tritium sink resulting from component replacement sets a maximum acceptable replacement frequency, unless novel tritium removal techniques capable of efficiently extracting most of the tritium within short periods are developed.

[9] Trapping site saturation can occur at similarly low dpa [21].

Acknowledgments

S. Meschini acknowledges the support from MITEI and Eni S.p.A. for his fellowship. The authors express their gratitude to the following individuals for their valuable feedback on this work: James Dark (CEA), Gabriele Ferrero (PoliTo), Thomas Schwarz-Selinger (IPP), Duc Nguyen-Manh (UKAEA). The authors also thank the participants of the 17th International Workshop on Hydrogen Isotopes in Fusion Reactor Materials for insightful discussions.

Appendix. Damage-induced traps

The input data for the damage-induced traps in tungsten are taken from [17] and reported in table A3.

Table A3. Input parameters for the damage-induced traps in FW, divertor, and VV. Data from [17]. The last neutron trap is never annealed.

	Parameters			
Trap	E_p (eV)	K ($m^{-3}dpa^{-1}$)	n_{max} (m^{-3})	E_A (eV)
Ion-induced	1.15	9×10^{26}	6.9×10^{25}	0.24
Neutron-induced #1	1.35	4.2×10^{26}	7.0×10^{25}	0.24
Neutron-induced #2	1.65	2.5×10^{26}	6.0×10^{25}	0.30
Neutron-induced #3	1.85	5.0×10^{26}	4.7×10^{25}	0.30
Neutron-induced #4	2.05	1×10^{26}	2.0×10^{25}	—

ORCID iDs

Samuele Meschini https://orcid.org/0000-0001-8014-903X
Rémi Delaporte-Mathurin https://orcid.org/0000-0003-1064-8882
George R. Tynan https://orcid.org/0000-0001-7461-4871
Sara E. Ferry https://orcid.org/0000-0002-7505-9571

References

[1] Ferry S., Abdallah M., Garcia-Diaz B., Humrickhouse P. and Young D. 2024 Fusion fuel cycles research objectives: results from the 2023 fusion fuel cycles workshop *Report 3002029371* EPRI (available at: www.epri.com/research/sectors/technology/results/3002029371)

[2] Ferry S., Abdallah M., Garcia-Diaz B., Humrickhouse P. and Young D. 2024 Fusion blankets research objectives: results from the 2023 fusion blankets workshop *Report 3002029373* EPRI (available at: www.epri.com/research/sectors/technology/results/3002029373)

[3] Meschini S., Ferry S.E., Delaporte-Mathurin R. and Whyte D.G. 2023 Modeling and analysis of the tritium fuel cycle for ARC-and STEP-class DT fusion power plants *Nucl. Fusion* **63** 126005

[4] Abdou M., Riva M., Ying A., Day C., Loarte A., Baylor L., Humrickhouse P., Fuerst T.F. and Cho S. 2020 Physics and technology considerations for the deuterium–tritium fuel cycle and conditions for tritium fuel self sufficiency *Nucl. Fusion* **61** 013001

[5] Coleman M., Hörstensmeyer Y. and Cismondi F. 2019 DEMO tritium fuel cycle: performance, parameter explorations and design space constraints *Fusion Eng. Des.* **141** 79–90

[6] Chen H., Pan L., Lv Z., Li W. and Zeng Q. 2016 Tritium fuel cycle modeling and tritium breeding analysis for CFETR *Fusion Eng. Des.* **106** 17–20

[7] Taylor N., Ciattaglia S., Cortes P., Iseli M., Rosanvallon S. and Topilski L. 2012 ITER safety and licensing update *Fusion Eng. Des.* **87** 476–81

[8] Federici G. *et al* 1998 Tritium inventory in the ITER PFC's: predictions, uncertainties, r&d status and priority needs *Fusion Eng. Des.* **39** 445–64

[9] Roth J. *et al* 2008 Tritium inventory in ITER plasma-facing materials and tritium removal procedures *Plasma Phys. Control. Fusion* **50** 103001

[10] Kirschner A., Borodin D., Droste S., Philipps V., Samm U., Federici G., Kukushkin A. and Loarte A. 2007 Modelling of tritium retention and target lifetime of the ITER divertor using the ERO code *J. Nucl. Mater.* **363** 91–95

[11] Roth J. *et al* 2005 Flux dependence of carbon erosion and implication for ITER *J. Nucl. Mater.* **337** 970–4

[12] Whyte D. 2009 On the consequences of neutron induced damage for volumetric fuel retention in plasma facing materials *J. Nucl. Mater.* **390** 911–5

[13] Ogorodnikova O., Tyburska B., Alimov V.K. and Ertl K. 2011 The influence of radiation damage on the plasma-induced deuterium retention in self-implanted tungsten *J. Nucl. Mater.* **415** S661–6

[14] Roth J. and Schmid K. 2011 Hydrogen in tungsten as plasma-facing material *Phys. Scr.* **2011** 014031

[15] Dark J., Delaporte-Mathurin R., Charles Y., Hodille E.A., Grisolia C. and Mougenot J. 2021 Influence of hydrogen trapping on WCLL breeding blanket performances *Nucl. Fusion* **61** 116076

[16] Arredondo R., Schmid K., Subba F. and Spagnuolo G. 2021 Preliminary estimates of tritium permeation and retention in the first wall of DEMO due to ion bombardment *Nucl. Mater. Energy* **28** 101039

[17] Dark J., Delaporte-Mathurin R., Schwarz-Selinger T., Hodille E.A., Mougenot J., Charles Y. and Grisolia C. 2023 Modelling neutron damage effects on tritium transport in tungsten *Nucl. Fusion* **64** 086026

[18] Doerner R., Tynan G. and Schmid K. 2019 Implications of pmi and wall material choice on fusion reactor tritium self-sufficiency *Nucl. Mater. Energy* **18** 56–61

[19] Schmid K., Schwarz-Selinger T., Arredondo Parra R., Theodorou A. and Lobo T.P. 2024 Implications of T loss in first wall armor and structural materials on T-self-sufficiency in future burning fusion devices *Nucl. Fusion* **64** 076056

[20] Hatano Y. *et al* 2013 Deuterium trapping at defects created with neutron and ion irradiations in tungsten *Nucl. Fusion* **53** 073006

[21] Schwarz-Selinger T. 2023 A critical review of experiments on deuterium retention in displacement-damaged tungsten as function of damaging dose *Mater. Res. Express* **10** 102002

[22] Pečovnik M., Markelj S., Kelemen M. and Schwarz-Selinger T. 2020 Effect of D on the evolution of radiation damage in W during high temperature annealing *Nucl. Fusion* **60** 106028

[23] Ogorodnikova O. 2015 Fundamental aspects of deuterium retention in tungsten at high flux plasma exposure *J. Appl. Phys.* **118** 074902

[24] Pressouyre G. and Bernstein I. 1978 A quantitative analysis of hydrogen trapping *Metall. Trans.* A **9** 1571–80

[25] Szost B.A., Vegter R.H. and Hydrogen P.E.J. 2013 Hydrogen-trapping mechanisms in nanostructured steels *Metall. Mater. Trans.* A **44** 4542–50

[26] Delaporte-Mathurin R., Dark J., Ferrero G., Hodille E.A., Kulagin V. and Meschini S. 2024 FESTIM: an open-source code for hydrogen transport simulations *Int. J. Hydrog. Energy* **63** 786–802

[27] Meschini S. and Delaporte-Mathurin R. 2024 Impact of trapping on tritium self-sufficiency and tritium inventories in fusion power plant fuel cycles - release for submission (https://doi.org/https://doi.org/10.5281/zenodo.13712716)

[28] Rosanvallon S., Benchikhoune M., Ciattaglia S., Uzan J.E., Gastaldi O., Na B. and Taylor N. 2011 Management of tritium in ITER waste *Fusion Sci. Technol.* **60** 855–60

[29] Matveev D. *et al* 2023 Tritium removal from JET-ILW after T and D–T experimental campaigns *Nucl. Fusion* **63** 112014

[30] Markelj S., Pečovnik M., Schwarz-Selinger T. and Kelemen M. 2022 The synergies between displacement damage creation and hydrogen presence: the effect of D ion energy and flux *Phys. Scr.* **97** 024006

[31] Klimenkov M., Dürrschnabel M., Jäntsch U., Lied P., Rieth M., Schneider H., Terentyev D. and Van Renterghem W. 2022 Microstructural analysis of W irradiated at different temperatures *J. Nucl. Mater.* **572** 154018

[32] Abdou M.A., Vold E., Gung C., Youssef M. and Shin K. 1986 Deuterium-tritium fuel self-sufficiency in fusion reactors *Fusion Technol.* **9** 250–85

[33] Crank J. 1979 *The Mathematics of Diffusion* (Oxford University Press)

[34] Hodille E. 2016 Study and modeling of the deuterium trapping in ITER relevant materials *PhD Dissertation* Universite D'Aix-Marseille

[35] Schmid K., Rieger V. and Manhard A. 2012 Comparison of hydrogen retention in W and W/TA alloys *J. Nucl. Mater.* **426** 247–53

[36] Kato D., Iwakiri H., Watanabe Y., Morishita K. and Muroga T. 2015 Super-saturated hydrogen effects on radiation damages in tungsten under the high-flux divertor plasma irradiation *Nucl. Fusion* **55** 083019

[37] Ogorodnikova O. and Sugiyama K. 2013 Effect of radiation-induced damage on deuterium retention in tungsten, tungsten coatings and eurofer *J. Nucl. Mater.* **442** 518–27

[38] Stopher M. 2017 The effects of neutron radiation on nickel-based alloys *Mater. Sci. Technol.* **33** 518–36

[39] Yamauchi Y., Yamada T., Hirohata Y., Hino T. and Muroga T. 2004 Deuterium retention in V–4Cr–4Ti alloy after deuterium ion irradiation *J. Nucl. Mater.* **329** 397–400

[40] Frauenfelder R. 1969 Solution and diffusion of hydrogen in tungsten *J. Vac. Sci. Technol.* **6** 388–97

[41] Ogorodnikova O., Roth J. and Mayer M. 2003 Deuterium retention in tungsten in dependence of the surface conditions *J. Nucl. Mater.* **313** 469–77

[42] Hodille E., Bernard E., Markelj S., Mougenot J., Becquart C., Bisson R. and Grisolia C. 2017 Estimation of the tritium retention in ITER tungsten divertor target using macroscopic rate equations simulations *Phys. Scr.* **2017** 014033

[43] Robertson W. 1977 Hydrogen permeation and diffusion in inconel 718 and incoloy 903 *Metall. Trans.* A **8** 1709–12

[44] Silva C., Song M., Leonard K., Wang M., Was G. and Busby J. 2017 Characterization of alloy 718 subjected to different thermomechanical treatments *Mater. Sci. Eng.* A **691** 195–202

[45] Lu X., Depover T. and Johnsen R. 2022 Evaluation of hydrogen diffusion and trapping in nickel alloy 625 by thermal desorption spectroscopy *Int. J. Hydrog. Energy* **47** 31673–83

[46] Hashizume K., Masuda J., Otsuka T., Tanabe T., Hatano Y., Nakamura Y., Nagasaka T. and Muroga T. 2007 Diffusional behavior of tritium in V–4CR–4TI alloy *J. Nucl. Mater.* **367** 876–81

[47] Kurzina I., Popova N., Kalashnikov M., Nikonenko E., Kazantseva L., Dement T., Klopotov A., Abzaev Y., Karakchieva N. and Koneva N. 2019 Peculiarities of structure and phase composition of V-TI-CR alloy obtained by sintering technique *J. Phys.: Conf. Ser.* **1145** 012051

[48] Esteban G., Pe na A., Urra I., Legarda F. and Riccardi B. 2007 Hydrogen transport and trapping in EUROFER'97 *J. Nucl. Mater.* **367** 473–7

[49] Chapman S. and Cowling T.G. 1990 *The Mathematical Theory of non-Uniform Gases: an Account of the Kinetic Theory of Viscosity, Thermal Conduction and Diffusion in Gases* (Cambridge University Press)

[50] Davey W.P. 1925 Precision measurements of the lattice constants of twelve common metals *Phys. Rev.* **25** 753

[51] Utoh H., Tobita K., Someya Y., Asakura N., Sakamoto Y., Hoshino K. and Nakamura M. 2015 Comparative evaluation of remote maintenance schemes for fusion DEMO reactor *Fusion Eng. Des.* **98** 1648–51

[52] Sorbom B. *et al* 2014 ARC: a compact, high-field, disassemblable fusion nuclear science facility and demonstration power plant *APS Division of Plasma Physics Meeting Abstracts* vol 2014 pp T8–005

[53] Gliss C., Bachmann C., Ciattaglia S., Drumm B., Camacho M.G., Moscato I., Mull T. and Palermo I. 2022 Integrated design of tokamak building concepts including ex-vessel maintenance *Fusion Eng. Des.* **177** 113068

[54] Bachmann C., Gliss C., Janeschitz G., Steinbacher T. and Mozzillo R. 2022 Conceptual study of the remote maintenance of the DEMO breeding blanket *Fusion Eng. Des.* **177** 113077

[55] Waganer L.M., Najmabadi F., Tillack M., Wang X. and El-Guebaly L. (A. Team) 2006 Design approach of the ARIES-AT power core and vacuum vessel cost assessment *Fusion Eng. Des.* **80** 181–200

[56] Ferrero G., Meschini S., Testoni R. and Zucchetti M. 2023 Exploration of ARC-class reactor vessel and divertor cooling system *Fusion Eng. Des.* **192** 113818

[57] Segantin S., Testoni R. and Zucchetti M. 2020 ARC reactor–neutron irradiation analysis *Fusion Eng. Des.* **159** 111792

[58] Whyte D., Delaporte-Mathurin R., Ferry S. and Meschini S. 2023 Tritium burn efficiency in deuterium–tritium magnetic fusion *Nucl. Fusion* **63** 126019

[59] Aiello G., Aubert J., Jonquères N., Puma A.L., Morin A. and Rampal G. 2014 Development of the helium cooled lithium lead blanket for DEMO *Fusion Eng. Des.* **89** 1444–50

[60] Aubert J., Aiello G., Jonquères N., Puma A.L., Morin A. and Rampal G. 2014 Development of the water cooled lithium lead blanket for DEMO *Fusion Eng. Des.* **89** 1386–91

[61] Van der Schaaf B., Tavassoli F., Fazio C., Rigal E., Diegele E., Lindau R. and LeMarois G. 2003 The development of eurofer reduced activation steel *Fusion Eng. Des.* **69** 197–203

[62] Ferrero G., Meschini S. and Testoni R. 2022 A preliminary cfd and tritium transport analysis for ARC blanket *Fusion Sci. Technol.* **78** 1–14

[63] Meschini S., Testoni R. and Zucchetti M. 2022 Development of an object-oriented, thermal-hydraulics model for ARC FLiBe loop safety assessment *Fusion Eng. Des.* **178** 113095

[64] Li-Puma A., Richou M., Magaud P., Missirlian M., Visca E. and Ridolfini V.P. 2013 Potential and limits of water cooled divertor concepts based on monoblock design as possible candidates for a DEMO reactor *Fusion Eng. Des.* **88** 1836–43

[65] Segantin S., Testoni R., Hartwig Z., Whyte D. and Zucchetti M. 2020 Optimization of tritium breeding ratio in ARC reactor *Fusion Eng. Des.* **154** 111531

[66] Bae J.W., Peterson E. and Shimwell J. 2022 ARC reactor neutronics multi-code validation *Nucl. Fusion* **62** 066016

[67] Boccaccini L. *et al* 2016 Objectives and status of eurofusion DEMO blanket studies *Fusion Eng. Des.* **109** 1199–206

[68] Del Nevo A. *et al* 2017 Wcll breeding blanket design and integration for DEMO 2015: status and perspectives *Fusion Eng. Des.***124** 682–6

[69] Aiello G., Aubert J., Forest L., Jaboulay J.-C., Puma A.L. and Boccaccini L. 2017 Design of the helium cooled lithium lead breeding blanket in cea: from TBM to DEMO *Nucl. Fusion* **57** 046022

[70] Theodorou A., Schmid K. and Schwarz-Selinger T. 2024 Annealing of hydrogen trap sites in displacement-damaged eurofer *Nucl. Mater. Energy* **38** 101595

[71] Zibrov M. and Schmid K. 2022 Reaction–diffusion simulations of hydrogen isotope trapping and release from cavities in tungsten, I: single cavity *Nucl. Mater. Energy* **30** 101121

[72] Zibrov M. and Schmid K. 2022 Reaction–diffusion simulations of hydrogen isotope trapping and release from cavities in tungsten, ii: Array of cavities *Nucl. Mater. Energy* **32** 101219

[73] Schwarz-Selinger T. personal communication

[74] Federici G. *et al* 1999 In-vessel tritium retention and removal in ITER *J. Nucl. Mater.* **266** 14–29

[75] Mueller D. 1997 Tritium removal from TFTR *J. Nucl. Mater.* **241** 897–901

[76] Roth J., Schwarz-Selinger T., Alimov V.K. and Markina E. 2013 Hydrogen isotope exchange in tungsten: Discussion as removal method for tritium *J. Nucl. Mater.* **432** 341–7

[77] Markelj S., Schwarz-Selinger T., Pečovnik M., Založnik A., Kelemen M., Čadež I., Bauer J., Pelicon P., Chromiński W. and Ciupinski L. 2019 Displacement damage stabilization by hydrogen presence under simultaneous w ion damage and d ion exposure *Nucl. Fusion* **59** 086050

[78] Hodille E., Bonnin X., Bisson R., Angot T., Becquart C., Layet J. and Grisolia C. 2015 Macroscopic rate equation modeling of trapping/detrapping of hydrogen isotopes in tungsten materials *J. Nucl. Mater.* **467** 424–31

[79] Hodille E., Založnik A., Markelj S., Schwarz-Selinger T., Becquart C., Bisson R. and Grisolia C. 2017 Simulations of atomic deuterium exposure in self-damaged tungsten *Nucl. Fusion* **57** 056002

[80] Delaporte-Mathurin R., Hodille E.A., Mougenot J., Charles Y. and Grisolia C. 2019 Finite element analysis of hydrogen retention in iter plasma facing components using festim *Nucl. Mater. Energy* **21** 100709

[81] Tyburska B., Alimov V.K., Ogorodnikova O., Schmid K. and Ertl K. 2009 Deuterium retention in self-damaged tungsten *J. Nucl. Mater.* **395** 150–5
[82] Gasparyan Y.M., Ogorodnikova O., Efimov V., Mednikov A., Marenkov E., Pisarev A., Markelj S. and Čadež I. 2015 Thermal desorption from self-damaged tungsten exposed to deuterium atoms *J. Nucl. Mater.* **463** 1013–6
[83] Založnik A., Markelj S., Schwarz-Selinger T., Ciupiński L., Grzonka J., Vavpetič P. and Pelicon P. 2016 The influence of the annealing temperature on deuterium retention in self-damaged tungsten *Phys. Scr.* **2016** 014031
[84] Hoen M 't., Tyburska-Püschel B., Ertl K., Mayer M., Rapp J., Kleyn A. and Zeijlmans van Emmichoven P. 2012 Saturation of deuterium retention in self-damaged tungsten exposed to high-flux plasmas *Nucl. Fusion* **52** 023008
[85] Ogorodnikova O. and Gann V. 2015 Simulation of neutron-induced damage in tungsten by irradiation with energetic self-ions *J. Nucl. Mater.* **460** 60–71